ISSN 1330-3651 (Print), ISSN 1848-6339 (Online) https://doi.org/10.17559/TV-20230731000838
Original scientific paper

Optimal PID Control for Precise Lubrication of Railway Turnout Dripper

Qian WANG*, Wei LI, Yuan-shuai LAN, Hua HE

Abstract: In order to reduce the influence of environment on the flow rate of lubricating oil and improve the accuracy of dripping oil, this paper developed an optimized proportional integral differential (PID) precision lubrication controller for railway switch locking hooks. The system models the temperature-dependent flow dynamics of biodegradable lubricants. An improved PID algorithm is proposed, which uses velocity feedback to enhance setpoint tracking and disturbance suppression. The simulation results show that the flow control accuracy is improved by 0.8% compared with the traditional PID method. Field tests over a temperature fluctuation range of –3 °C to 35 °C validate the effectiveness and robustness of the method for maintaining a constant drop rate. This research enables adaptive, environmentally friendly lubrication to reduce friction and ensure the operability of railway switch.

Keywords: disturbance suppression; fixed-point tracking; modeling; PID; switch lock hook; velocity feedback

1 INTRODUCTION

The way of controlling switches has experienced the development process from manual to electric. High-speed trains will have a strong impact on switches, so the switch state will be locked by locking hooks in actual use [1-3], otherwise the train is easy to derail. If the locking device is not well lubricated, the following two situations will occur: first, the locking iron will develop abrasion marks, resulting in increased friction, and the locking hook cannot automatically fall, resulting in blocking failure; second, the friction of the slide plate will increase, and the operation resistance of the switch will increase, and the switch will appear stuck and idling, which seriously threatens the safety of rail transportation [4-6]. Therefore, accurate and efficient oil injection is a necessary condition to ensure the normal operation of the lock hook [7-8]. In China, the main ways to add lubricating oil to the switch lock hook include manual oiling, rail block refueling, and the mechanical thimble with the switch to control the fixed oil tank dripping [9]. In recent years, with the rapid development of China's high-speed railway, the electric control refueling method has been realized [10]. This method adopts power line network power supply, carries out modular design, and realizes cellular layout management through wired network. It has advantages such as easy installation and remote control, but there are still many defects in power consumption, oil quantity management and drip speed control. One of the typical applications is the cellular refueling system based on the Internet of Things, which uses temperature feedback control, but in the actual application, the ambient temperature does not change significantly in a short time, so it cannot achieve high-precision flow rate, leads to a lack of precise control, as well as adaptability to the environment. Therefore, the control of drip oil flow rate is one of the main research directions. Literature proposes a velocity foresight algorithm to connect the velocity between path segments and to fit a large number of parameter curves of small line segments [11], so as to achieve continuous control of the velocity. However, this algorithm has poor stability and is easily affected by environmental factors. In literature [12], an interpolation algorithm was proposed to discrete the moving trajectory of a moving object into a large number of small line segments connected from end to end to improve the precision of speed control. However, this algorithm is an open-loop control, and the control process is more dependent on the initial value. In literature [13], a climbing evolutionary algorithm is proposed. The idea is to move forward continuously, compare the time before and after, calculate the differences, so as to distinguish the velocity change and adjust the constant velocity. The calculation process of this algorithm is prone to premature convergence and large deviation. In literature [14], a fuzzy control algorithm is proposed, which obtains the precise value of the controlled velocity by sampling, and then compares the quantity with the given value to obtain the error signal, and identifies the error signal to determine the stable state of the velocity. The boundary conditions of this algorithm are more complicated and the calculation amount is larger. Literature proposes a neural network control algorithm, which uses the neural network crossover structure to query the optimal speed value and output the process as the control quantity [15]. Literature proposes a speed control genetic algorithm to build an initial population and iteratively search for the optimal value [16]. Literature proposes a PID control algorithm [17], which realizes the stability of speed control through closed-loop control mechanism, but the control accuracy is weak and it is not robust. PID control theory has an important application in the control system, whose core idea is to adjust the deviation of the system through the proportion, integral and differential three links to achieve the stability and accuracy of the system [18]. The PID control theory can be optimized in many ways: using the parameter self-tuning technology of the PID controller [19]. The optimal control effect of PID controller is realized by automatically adjusting the proportional coefficient Kp, integral constant Ti and differential constant Td. Integrating saturation is introduced to prevent oscillations. When the output of the PID controller reaches saturation, the cumulative value of the integral term is recalculated to a more ideal value to avoid excessive cumulative value of the integral term resulting in system oscillation. Variable integral PID is adopted [20]. The speed of the integral term is changed according to the deviation of the system. The greater the deviation [21], the slower the integral is. The smaller the deviation, the faster the integration. This can better adapt to the system control requirements under different deviation sizes. Optimization in combination with

other control theories and techniques such as fuzzy control, neural network, genetic algorithm and so on [22]. These technologies can further improve the performance and robustness of PID controllers, enabling them to better adapt to complex and changing industrial field environments. In this paper, based on the existing PID control fueling method, an adaptive control system is constructed to optimize the flow rate of lubricating oil, and speed feedback is used to enhance setpoint tracking and disturbance suppression, and the dynamic relationship of the drip process is combined to improve the control accuracy of oil flow rate.

2 RESEARCH METHOD

2.1 Basic Model

The lubricating oil selected from a company biodegradable lubricating oil, with natural degradation performance, does not pollute the environment. The property values are shown in Tab. 1.

Table 1 Lubricating oil material properties

event	parameter	event	parameter
Lubricating oil type	NSF-H-1	Flash point / °C	264
40 °C Kinematic viscosity η / mm^2/s	142.0	Pour point / °C	–40
100 °C Kinematic viscosity η / mm^2/s	27.0	density / kg·m^{-3}	0.894

The relationship between lubricating oil density and temperature can be expressed as follows:

$$\rho = m + nT \tag{1}$$

where, m, n is the correction coefficient; T is temperature; The correction coefficient in Eq. (1) is obtained by fitting the least square method [23]: m = 0.9044, n = –0.00056. Put into Eq. (1):

$$\rho = 0.9044 - 0.00056T \tag{2}$$

A lubricating oil flow dynamic model [24-25] was established to discuss the mechanism of temperature affecting fluid flow. The dynamic relation of lubricating oil flow can be expressed as:

$$Q_V = f(k, \Delta p, T) \tag{3}$$

where, k is the coefficient related to the flow pipe geometry; Δp is the pressure; T is temperature.

The kinematic viscosity can be calculated by the Walser equation as follows:

$$v_T = 10^{\left[10^{(A - B\lg nT + Kn)}\right]} - C \tag{4}$$

where, v_T is kinematic viscosity at temperature T, °C; A, B and C are lubricating oil coefficient; K is the absolute temperature 273.15 °C.

Calculated lubricating oil coefficient A = 6.046, B = 2.289. C Take the experience value 0.6. This value is substituted into Eq. (5) to obtain:

$$v_T = 10^{\left[10^{(6.046 - 2.289\lg nT + 273.15n)}\right]} - 0.6 \tag{5}$$

Based on the relationship between hydrodynamic viscosity and kinematic viscosity, it can be obtained:

$$\eta = v \times \rho \tag{6}$$

where, v is kinematic viscosity, centipoise, ρ is lubricating oil density, g/cc, η is dynamic viscosity, pars.

Eq. (5) is substituted into Eq. (6) to obtain the dynamic viscosity:

$$\eta = v_T \rho = \left\{10^{\left[10^{(6.046 - 2.289\lg nT + 273.15n)}\right]} - 0.6\right\}\rho \tag{7}$$

Newton viscous fluid flow model is adopted, the lubricating oil is incompressible, and the edge effect is ignored. The lubricating oil flow model in the oil outlet pipeline is regarded as the laminar flow velocity relation, and the laminar flow velocity is:

$$Q_V = \int_0^{r_0} u \cdot 2\pi r dr = \frac{\pi \Delta p}{8\eta l} r^4 = k\frac{\Delta p}{\eta} \tag{8}$$

k is the coefficient related to the flowpipe geometry, namely: $k = \dfrac{\pi r^4}{8l} = 0.003925$ mm^3. Substituting Eq. (2) and (7) into Eq. (8), we can get:

$$Q_V = \frac{0.003925\Delta p}{\left\{10^{\left[10^{(6.046 - 2.289\lg nT + 273.15n)}\right]} - 0.6\right\}} \cdot \frac{1}{(0.9044 - 0.00056T)} \tag{9}$$

In Eq. (8) and Eq. (9), u is the laminar flow velocity; r is the outlet pipe radius, mm; η is for dynamic viscosity, pars. ρ is lubricating oil density, kg/m^3; l is the length between the oil tank and the outlet pipe nozzle, which is 100 mm in the test; Δp pressure difference between the highest liquid level of the tank and the nozzle of the outlet pipe, pa; A, B and C are lubricating oil coefficients.

2.2 Improved PID Algorithm Based Model

PID is a feedback closed-loop control algorithm, which is composed of three parameters, namely, proportional parameter, integral parameter and differential parameter [23-25]. In the traditional control system, it is used to adjust the motor speed, adjust the constant temperature, control switch operation, etc. [26]. Proportional parameters, integral parameters and differential parameters are calculated as follows [27-29]:

$$P_o = K_p U_{in} \tag{10}$$

$$I_o = K_p \frac{1}{T_i}\int_0^t U_{in}(t)dt \tag{11}$$

$$D_o = K_p T_d \frac{\mathrm{d}\left(U_{in}(t) - U_{in}(t-1)\right)}{\mathrm{d}t} \tag{12}$$

Under PID control, total output:

$$U_{out} = P_o + I_o + D_o \tag{13}$$

That is:

$$U_{out} = K_p U_{in} + K_p \frac{1}{T_i}\int_0^t U_{in}(t)\,dt + \\ + K_p T_d \frac{d\left(U_{in}(t) - U_{in}(t-1)\right)}{dt} \tag{14}$$

where, U_{out} is the output under PID control, that is, position PID [30]. In this control process, the controlled part can effectively enter the steady state quickly and with high control accuracy, but the proportional coefficient of PID is fixed and cannot change with the flow rate [31], so that the operation of the controlled part always lags behind the control command. Therefore, an improved PID algorithm is proposed to introduce the drip flow rate Q into the PID control process. Speed feedback is used to enhance set-point tracking and disturbance suppression to enhance the stability of constant flow control systems. The realization process is to record the flow rate of two adjacent times, calculate the difference, and then pass the difference to the PID algorithm in the traditional form. The implementation process is shown in Fig. 1.

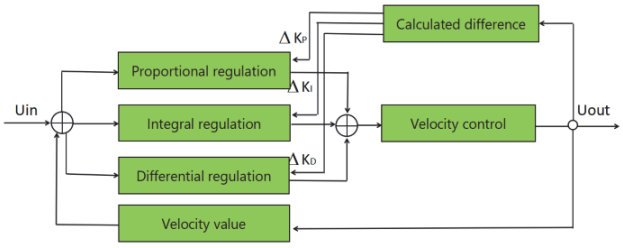

Figure 1 Block diagram of constant velocity control system with improved PID algorithm

In Fig. 1, the input-output relationship is expressed as follows:

$$U_{out}(i) = U_{out}(i-1) + \Delta U_{out}(i) = \\ = U_{out}(i-1) + K_p\left(U_{in}(i) - U_{in}(i-1) + \right. \\ \left. + \frac{T}{I}U_{in}(i) + D\frac{U_{in}(i) - 2U_{in}(i-1) + U_{in}(i-2)}{T}\right) \tag{15}$$

where, $U_{out}(i)$ is the output of the improved PID algorithm, which is only related to the increment of the controlled quantity. After the introduction of velocity variation, the output of the whole system is only related to the velocity variation, and has nothing to do with the location of the system environment, which greatly enhances the control accuracy of the system. The implementation logic of improved PID algorithm software is shown in Fig. 2.

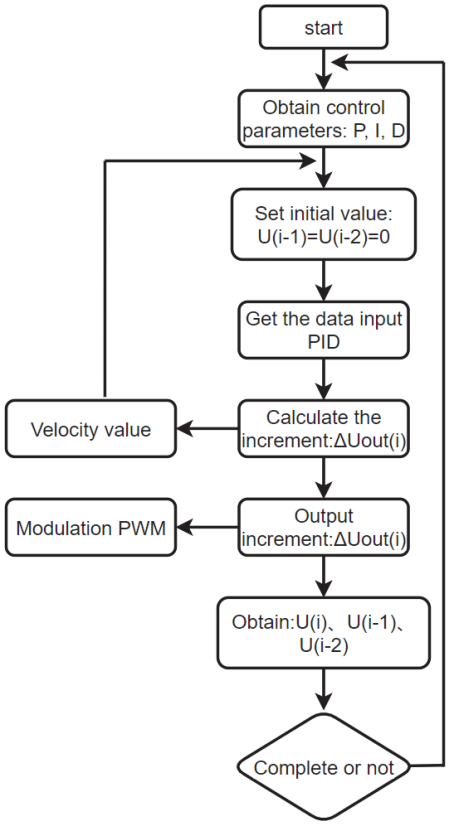

Figure 2 Improved PID algorithm software implementation logic

The PID gain adjustment process steps are as follows [32-35]:

1. When the output does not oscillate, increase the proportional gain *P*.
2. Determine the integral time constant *Ti*. After the proportional gain *P* is determined, a large initial value of the integral time constant *Ti* is set, and then *Ti* is gradually reduced until the system oscillates, and then vice versa, *Ti* is gradually increased until the system oscillation disappears. Record *Ti* at this time and set the integral time constant *Ti* of PID to 120% - 150% of the current value.
3. Determine the differential time constant *Td*. The setting method is the same as that of *P* and *Ti*, taking 30% of the value without oscillation.
4. The system is connected with no-load and on-load, and the PID parameters are fine-tuned until they meet the requirements.

3 EXPERIMENT AND RESULTS

3.1 Experimental Design

3.1.1 System Hardware Design

The structure diagram of the control system of the drip device is shown in Fig. 3. The main controller uses STM32L431RCT6 as the core, which is connected with external temperature sensor, liquid level detection sensor, metal sensor, flow rate sensor, expansion interface, oil pump and human-computer interaction interface. Expansion interface external wireless communication module.

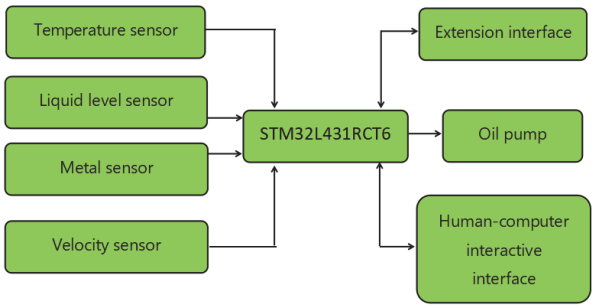

Figure 3 Block diagram of control system

Temperature sensor adopts single-bus 12-bit digital temperature sensor DS18B20 chip; the liquid level sensor adopts ±1 mm high-precision capacitive sensor, model XL2524-NPN; metal sensor adopts high sensitivity magnetic sensor, model GL-12F; the flow rate sensor adopts the principle of Doppler flow rate measurement, the measurement accuracy is 3% F.S, the model is H8000B; the LORA communication module model is ZHC0941.

3.1.2 System Software Design

The system software design idea is shown in Fig. 4. After the system is running, the first step is to initialize each module, including: SCM clock configuration, interrupt vector nested configuration, GPIO configuration, serial communication configuration, IIC configuration, Flash read and write configuration, key initialization, oil control pump module initialization, temperature sensor initialization, PID algorithm initialization and OLED display initialization. Step 2 Query the Flash storage value and collect the velocity sensor data at a sampling interval of 200 ms.

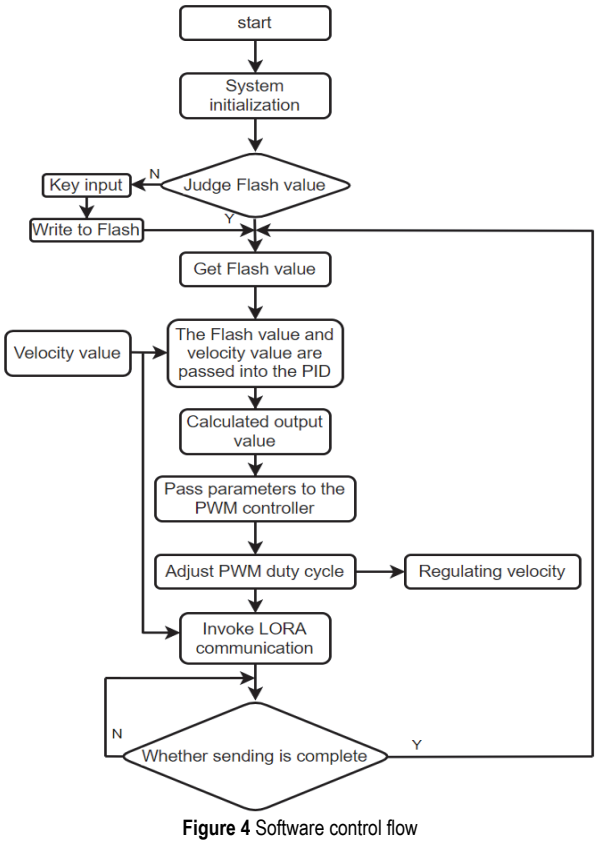

Figure 4 Software control flow

The third step is to pass the sampled value and Flash stored value into the improved PID algorithm to calculate the PWM wave regulation duty ratio data. In the fourth step, the difference between the current sampling value and that of the previous step is made, and the calculated difference is passed into the improved PID algorithm to calculate the PWM wave regulation duty ratio data. The fifth step output PWM wave, so as to control the pump velocity. In the design, the flow rate sensor adopts the periodic measurement mode and uses timer 1 to set the sampling rate. The sampling frequency is 20 Hz, and 20 times of data acquisition are obtained each time. The maximum and minimum values in the 20 times are removed, and then the average value of the remaining values is calculated as the output value, so as to reduce the impact of the sudden error value in the measurement on the measurement results. Timer 2 and timer 3 were used to set the PID calculation period and PWM wave output period, which were 200 ms and 150 ms respectively.

PID optimization algorithm code is as follows:

```
int32_tSpdPIDCalc(float NextPoint)
{
float iError,iIncpid;
iError = (float)sPID.SetPoint – NextPoint;
if((iError < 0.05f )&& (iError > –0.05f))
iError = 0.0f;
iIncpid = (sPID.Proportion*iError) –
(sPID.Integral*sPID.LastError) +
(sPID.Derivative*sPID.PrevError);
sPID.PrevError = sPID.LastError;
sPID.LastError = iError;
return(iIncpid);
```

In the program, sPID.LastError is the current error, and sPID.PrevError is the last error. sPID.Proportion is the constant of proportion; sPID.Integral is the integral constant; sPID.Derivative is a differential constant; sPID.SetPoint sets the speed target.

3.2 Experimental Results and Discussion

3.2.1 Algorithm Test

In order to improve system reliability, MATLAB simulation is used to verify the performance of related parameters, so as to verify the actual performance of the improved PID algorithm [36-38]. In the simulation test, the velocity value is set as 0.1 cm/s, and after the control system is started, the velocity value will be stabilized at this set value. Multiple groups of KP, KI and KD values were selected for the experiment. KP is 35, 40, 45, and the integral and differential coefficients are 0. The waveform of simulation test under different proportional coefficients is shown in Fig. 5.

As can be seen from Fig. 5, when the scale coefficient is 40, the system tends to the set value more. System rise time < 3 ms; Regional stability time < 10 ms; Overshoot percentage 50%. On the basis of Fig. 5, integral operation was added, integral coefficients KI were set as: 650000, 700000 and 750000 respectively, and differential coefficients were set as 0. The output waveform of simulation test was shown in Fig. 6.

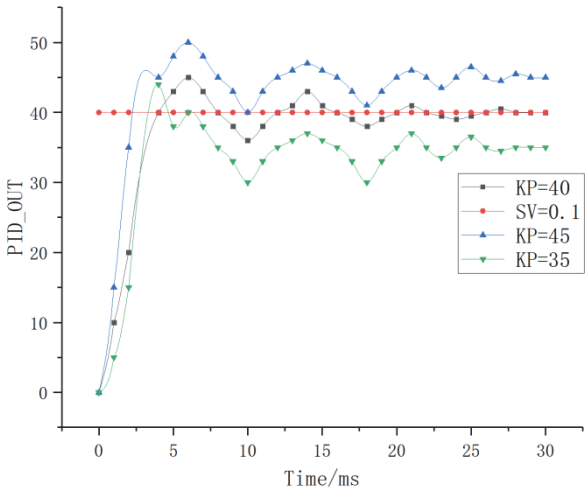

Figure 5 Output waveform under different proportional coefficients

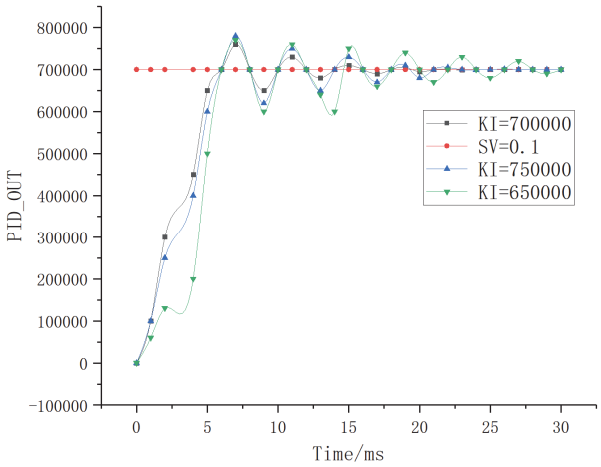

Figure 6 Output waveform of adding integral operation

As can be seen from Fig. 6, after increasing the integral coefficient, the error between the output waveform and the steady state becomes smaller and smaller. When the integral coefficient is 7000000, the error between the output waveform and the steady state is the smallest. System rise time < 7 ms; Regional stability time < 10 ms. On the basis of Fig. 6, differential operation is added, and differential coefficient KD is set as 600, 800 and 1100 respectively. The output waveform of simulation test is shown in Fig. 7.

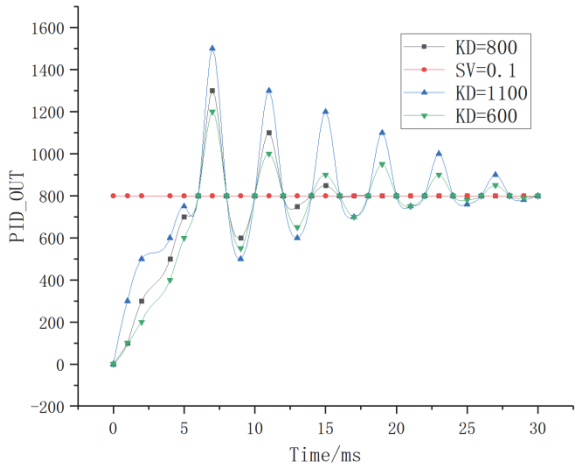

Figure 7 Output waveform of adding differential operation

As can be seen from Fig. 7, the output waveform enters the set value more quickly. When the differential coefficient is 800, the system enters the stable state at the earliest. As can be seen from Fig. 5 to 7, the system is most stable when KP, KI and KD are 40, 700,000 and 800 respectively. The system is powered on and starts to work to obtain the preset velocity. When the velocity collected from the velocity sensor reaches the preset value, the velocity increases, decreases rapidly, and stabilizes at the preset value. The data acquisition method is printed by the serial assistant. The experimental waveform is shown in Fig. 8.

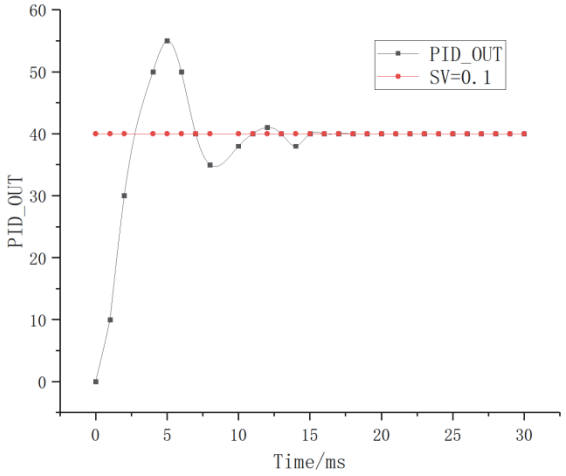

Figure 8 PID output with different inputs

As can be seen from Fig. 8, it takes less than 15 mS for the output to stabilize. System rise time < 5 ms; The overshoot percentage is 50%. Modeling simulation test was carried out on the improved PID algorithm control system. It can be seen from the test results that the flow rate control accuracy was increased from 3.5% to 2.7%, and the accuracy was increased by 0.8%. And the system can produce a quick response, can quickly enter a stable state, can withstand greater interference. The comparison of flow rate before and after PID algorithm is applied in the control system is shown in Fig. 9.

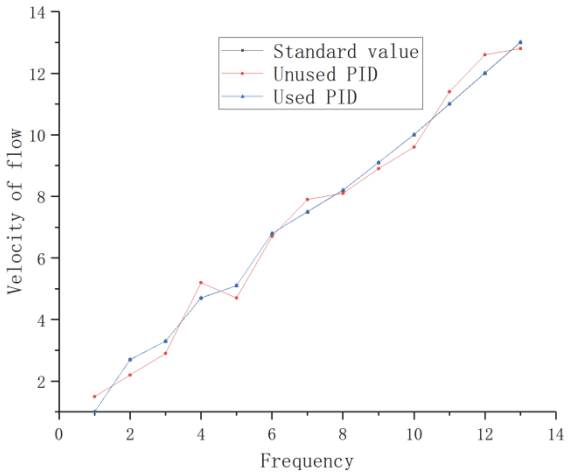

Figure 9 Comparison of velocity before and after PID algorithm is applied

In Fig. 9, the actual flow rate using PID algorithm is very close to the set standard value, while the actual flow rate without PID algorithm jumps up and down the

standard value and fluctuates greatly. The data table is shown in Tab. 2 below:

Table 2 Comparison before and after optimization of PDI algorithm

Item	Before optimization	post-optimization
Rise time / ms	> 27	< 7
Percentage overshoot / %	> 80	< 50
Settling time / ms	> 300	< 15
Steady-state error	> 0.50	< 0.01

3.2.2 Field Test

After the algorithm modeling is programmed and installed on the physical platform, the above simulation verification results can be obtained for the physical system. The physical platform is shown in Fig. 10.

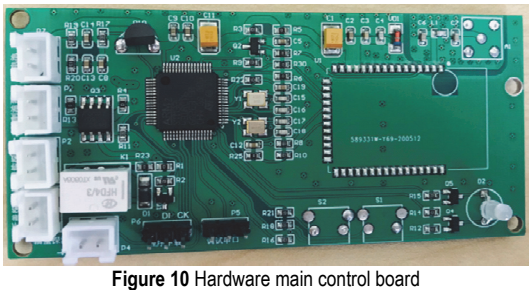

Figure 10 Hardware main control board

The shell of the physical device is made of metal steel, which is resistant to fall and earthquake resistance. It is equipped with the main control system of the oil dropper and all the circuits and the fuel tank. The circuit system is sealed, waterproof and dust-proof by silica gel. A metal sensor at the front of the nozzle detects whether the hook is extended. See Fig. 11.

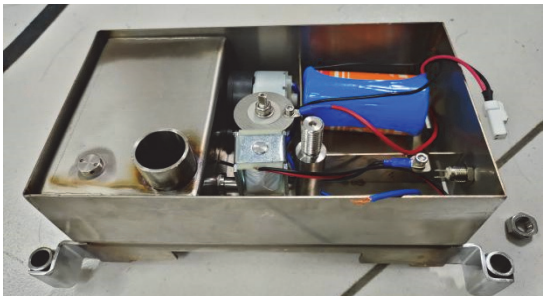

Figure 11 Physical device drops oil

The test sites were selected in northeast Sichuan, Chengdu Plain in central Sichuan and southern Sichuan. Track types are common rail switch hook and high-speed rail two, as shown in Tab. 3. The test temperature ranges from –3 ℃ to + 35 ℃.

Table 3 Test conditions

Test site	Hook type	Ambient temperature / ℃
Middle section of Chengdu-Chongqing Railway	General railway	–1 ~ +30
Guangyuan section of Baocheng Railway	General railway	–3 ~ +30
Yibin section of Chengdu-Guizhou high-speed railway	High-speed railway	+3 ~ +35

Fig. 12 shows the curve relationship between ambient temperature and dripping time in the three places.

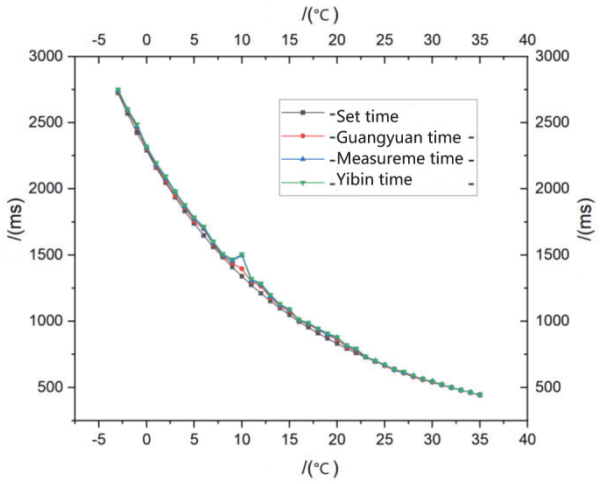

Figure 12 Use of dripping equipment tested in three places

As can be seen from Fig. 12, with the increase of ambient temperature, the dripping velocity remains stable, and the dripping velocity remains basically constant even in different regions. This greatly reduces the influence of environmental factors on the drip process, improves the stability of accurate drip and saves oil.

3.2.3 Drip Dynamics Analysis

Dynamic analysis is the most direct and simplest method to study the changes of fluid flow process. It studies the non-equilibrium system with fluid properties changing with temperature, pressure and density, and mainly studies the factors affecting velocity and dynamic relationship in the process of fluid flow. The fluid constant and correction coefficient can be obtained under the set boundary conditions by the kinetic study. Combined with the measured data, Eq. (9) was modified to obtain the dynamic relationship of the oil dripping process in the three places as follows:

Guangyuan Segment (Temperature range: –3 ℃ to +30 ℃):

$$Q_V = \frac{0.03925\Delta p}{\left\{10^{\left[10^{(6.046-2.289\lg nT+273.15n)}\right]}-0.586\right\}} \cdot \frac{1}{(0.9044-0.00056T)} \tag{16}$$

Middle section (Temperature range: –1℃ to +30℃):

$$Q_V = \frac{0.03925\Delta p}{\left\{10^{\left[10^{((6.246-2.189\lg nT+273.15n)}\right]}-0.616\right\}} \cdot \frac{1}{\times(0.9044-0.00056T)} \tag{17}$$

Yibin Section (Temperature range: +3 ℃ to +35 ℃):

$$Q_V = \frac{0.03925\Delta p}{\left\{10^{\left[10^{(6.317-2.089lg\,n\mathrm{T}+273.15\mathrm{n})}\right]}-0.685\right\}} \cdot \frac{1}{(0.9044-0.00056T)} \tag{18}$$

Considering practical application, the atmospheric pressure of lubricating oil working environment is basically less than 40 MPa, and the influence of pressure viscosity is ignored.

4 CONCLUSION

The optimized Proportional Integral differential (PID) precision lubrication controller for railway switch locks combines coupling lubricating oil dynamics modeling with adaptive PID control, uses speed feedback to enhance set point tracking and disturbance suppression, and achieves adaptive control system and more environmentally friendly oil drips to reduce friction and ensure the operability of railway switch.

Acknowledgements

Foundation Information: Humanities and Social Science Fundof Ministry of Education, China; 21XJA630004.

5 REFERENCES

[1] Cao, Y., An, Y., Su, S., Xie, G., & Sun, Y. (2022). A statistical study of railway safety in China and Japan 1990 - 2020. *Accident Analysis & Prevention, 175*, 106764. https://doi.org/10.1016/j.aap.2022.106764

[2] Kour, R., Patwardhan, A., Thaduri, A., & Karim, R. (2023). A review on cybersecurity in railways. *Proceedings of the Institution of Mechanical Engineers, Part F: Journal of Rail and Rapid Transit, 237*(1), 3-20. https://doi.org/10.1177/09544097221089389

[3] Huang, Y., Zhang, Z., Tao, Y., & Hu, H. (2022). Quantitative risk assessment of railway intrusions with text mining and fuzzy Rule-Based Bow-Tie model. *Advanced Engineering Informatics, 54*, 101726. https://doi.org/10.1016/j.aei.2022.101726

[4] Zhou, S., Chen, B., & Liu, Q. (2022, November). Design of locking control system for vehicle charging port. *International Symposium on Robotics, Artificial Intelligence, and Information Engineering (RAIIE 2022), 12454*, 385-390. https://doi.org/10.1117/12.2658850

[5] Nakhal Akel, A. J., Di Gravio, G., Fedele, L., & Patriarca, R. (2022). Learning from Incidents in Socio-Technical Systems: A Systems-Theoretic Analysis in the Railway Sector. *Infrastructures, 7*(7), 90. https://doi.org/10.3390/infrastructures7070090

[6] Meng, Q., Wen, W., Bai, Y., & Liu, Y. (2022). A fault detection method for electrohydraulic switch machine based on oil-pressure-signal-sectionalized feature extraction. *Entropy, 24*(7), 848. https://doi.org/10.3390/e24070848

[7] Fang, J., Chen, R., Hu, C., Chen, J., Xu, J., & Wang, P. (2022). Simulation analysis of high-speed turnout point rail switching force considering influence of external locking device. *Proceedings of the Institution of Mechanical Engineers, Part F: Journal of Rail and Rapid Transit, 236*(1), 48-57. https://doi.org/10.1177/09544097211001152

[8] Wen, W., Liu, Y., Bai, Y., & Meng, Q. (2023). A feature pseudo-fusion method for intelligent fault diagnosis of electro-hydraulic switch machine inspired by contrastive learning. *Proceedings of the Institution of Mechanical Engineers, Part F: Journal of Rail and Rapid Transit*.https://doi.org/10.1177/09544097231165093

[9] Lu, C. & Cai, C. (2020). Overview on safety management and maintenance of high-speed railway in China. *Transportation Geotechnics, 25*, 100397. https://doi.org/10.1016/j.trgeo.2020.100397

[10] Falahati, A. & Shafiee, E. (2022). Improve safety and security of intelligent railway transportation system based on balise using machine learning algorithm and fuzzy system. *International Journal of Intelligent Transportation Systems Research*, 1-15. https://doi.org/10.1007/s13177-021-00274-1

[11] Zhang, C., Gao, G., Zhao, C., Li, L., Li, C., & Chen, X. (2022). Research on 4WS Agricultural Machine Path Tracking Algorithm Based on Fuzzy Control Pure Tracking Model. *Machines, 10*(7), 597. https://doi.org/10.3390/machines10070597

[12] Sharma, S., Chakraborty, S., Saha, A. K., Nama, S., & Sahoo, S. K. (2022). mLBOA: A modified butterfly optimization algorithm with lagrange interpolation for global optimization. *Journal of Bionic Engineering, 19*(4), 1161-1176. https://doi.org/10.1007/s42235-022-00175-3

[13] Seck-Tuoh-Mora, J. C., Escamilla-Serna, N. J., Montiel-Arrieta, L. J., Barragan-Vite, I., & Medina-Marin, J. (2022). A global neighborhood with hill-climbing algorithm for fuzzy flexible job shop scheduling problem. *Mathematics, 10*(22), 4233. https://doi.org/10.3390/math10224233

[14] Pan, Y., Wu, Y., & Lam, H. K. (2022). Security-based fuzzy control for nonlinear networked control systems with DoS attacks via a resilient event-triggered scheme. *IEEE Transactions on Fuzzy Systems, 30*(10), 4359-4368. https://doi.org/10.1109/TFUZZ.2022.3148875

[15] He, F. & Ye, Q. (2022). A bearing fault diagnosis method based on wavelet packet transform and convolutional neural network optimized by simulated annealing algorithm. *Sensors, 22*(4), 1410. https://doi.org/10.3390/s22041410

[16] Anwaar, A., Ashraf, A., Bangyal, W. H. K., & Iqbal, M. (2022). Genetic Algorithms: Brief review on Genetic Algorithms for Global Optimization Problems. *2022 Human-Centered Cognitive Systems (HCCS)*, 1-6. https://doi.org/10.1109/HCCS55241.2022.10090327

[17] Kose, O. & Oktay, T. (2022). Hexarotor Yaw Flight Control with SPSA, PID Algorithm and Morphing. *International Journal of Intelligent Systems and Applications in Engineering, 10*(2), 216-221.

[18] Lin, J., Zheng, R., Zhang, Y., Feng, J., Li, W., & Luo, K. (2022). CFHBA-PID algorithm: Dual-loop PID balancing robot attitude control algorithm based on complementary factor and honey badger algorithm. *Sensors, 22*(12), 4492. https://doi.org/10.3390/s22124492

[19] Wang, W., Wu, K., Zhang, Y., Wang, M., Zhang, C., & Chen, L. (2022). The development of an electric-driven control system for a high-speed precision planter based on the double closed-loop fuzzy PID algorithm. *Agronomy, 12*(4), 945. https://doi.org/10.3390/agronomy12040945

[20] Yang, R., Wang, Z., Shang, S., Zhang, J., Qing, Y., & Zha, X. (2022). The design and experimentation of EVPIVS-PID harvesters' header height control system based on sensor ground profiling monitoring. *Agriculture, 12*(2), 282. https://doi.org/10.3390/agriculture12020282

[21] Qi, Y., Jing, H., & Wu, X. (2022). Variable Structure PID Controller for Satellite Attitude Control Considering Actuator Failure. *Applied Sciences, 12*(10), 5273. https://doi.org/10.3390/app12105273

[22] Jamil, A. A., Tu, W. F., Ali, S. W., Terriche, Y., & Guerrero, J. M. (2022). Fractional-order PID controllers for temperature control: a review. *Energies, 15*(10), 3800.

https://doi.org/10.3390/en15103800
[23] Wang, Z. & Zhang, J. (2022). Incremental PID Controller-Based Learning Rate Scheduler for Stochastic Gradient Descent. *IEEE Transactions on Neural Networks and Learning Systems*.
[24] Liu, M., Zhang, H., Zhang, Y., & Yuan, C. (2022). Design and Performance Analysis of ZYNQ Based Incremental PID-PWM Controller. 2022 *IEEE International Conference on Electrical Engineering, Big Data and Algorithms (EEBDA)*, 1123-1126. https://doi.org/10.1109/EEBDA53927.2022.9744964
[25] Omar, O. A., Marei, M. I., & Attia, M. A. (2023). Comparative Study of AVR Control Systems Considering a Novel Optimized PID-Based Model Reference Fractional Adaptive Controller. *Energies, 16*(2), 830. https://doi.org/10.3390/en16020830
[26] Veerasamy, V., Wahab, N. I. A., Ramachandran, R., Othman, M. L., Hizam, H., Kumar, J. S., & Irudayaraj, A. X. R. (2022). Design of single-and multi-loop self-adaptive PID controller using heuristic based recurrent neural network for ALFC of hybrid power system. *Expert Systems with Applications, 192*, 116402. https://doi.org/10.1016/j.eswa.2021.116402
[27] Shuprajhaa, T., Sujit, S. K., & Srinivasan, K. (2022). Reinforcement learning based adaptive PID controller design for control of linear/nonlinear unstable processes. *Applied Soft Computing, 128*, 109450. https://doi.org/10.1016/j.asoc.2022.109450
[28] Lui, D. G., Petrillo, A., & Santini, S. (2022). Leader tracking control for heterogeneous uncertain nonlinear multi-agent systems via a distributed robust adaptive PID strategy. *Nonlinear Dynamics, 108*(1), 363-378. https://doi.org/10.1007/s11071-022-07240-w
[29] Hair Jr, J. F., Sarstedt, M., Ringle, C. M., & Gudergan, S. P. (2023). *Advanced issues in partial least squares structural equation modeling*. saGe publications. https://doi.org/10.1007/978-3-319-57413-4_15
[30] Liu, J., Ni, H., Zhou, R., Li, X., Xing, Q., & Pan, G. (2023). A simulation analysis of ball bearing lubrication characteristics considering the cage clearance. *Journal of Tribology, 145*(4), 044301. https://doi.org/10.1115/1.4056358
[31] Joseph, S. B., Dada, E. G., Abidemi, A., Oyewola, D. O., & Khammas, B. M. (2022). Metaheuristic algorithms for PID controller parameters tuning: Review, approaches and open problems. *Heliyon, 8*(5). https://doi.org/10.1016/j.heliyon.2022.e09399
[32] Han, S. Y., Dong, J. F., Zhou, J., & Chen, Y. H. (2022). Adaptive fuzzy PID control strategy for vehicle active suspension based on road evaluation. *Electronics, 11*(6), 921. https://doi.org/10.3390/electronics11060921
[33] Singhal, K., Kumar, V., & Rana, K. P. S. (2022). Robust trajectory tracking control of non-holonomic wheeled mobile robots using an adaptive fractional order parallel fuzzy PID controller. *Journal of the Franklin Institute, 359*(9), 4160-4215. https://doi.org/10.1016/j.jfranklin.2022.03.043
[34] Lei, G., Chang, X., Tianhang, Y., & Tuerxun, W. (2022). An improved mayfly optimization algorithm based on median position and its application in the optimization of PID parameters of hydro-turbine governor. *IEEE Access, 10*, 36335-36349. https://doi.org/10.1109/ACCESS.2022.3160714
[35] Štampar, M. & Fertalj, K. (2022). Applied Machine Learning in Recognition of DGA Domain Names. *Computer Science and Information Systems, 19*(1), 205-227. https://doi.org/10.2298/CSIS210104046S
[36] Micheletto, M. J., Chesñevar, C. I., & Santos, R. M. (2022). A novel approach for sEMG gesture recognition using resource-constrained hardware platforms. *Computer Science and Information Systems, 19*(3), 1199-1212. https://doi.org/10.2298/CSIS220228025M
[37] Petrović, A., Biserčić, A., Delibašić, B., & Milenković, D. (2022). A Machine Learning approach for learning temporal point process. *Computer Science and Information Systems, 19*(2), 1007-1022. https://doi.org/10.2298/CSIS210609016P
[38] Alexiev, K. & Vakarelsky, T. (2022). Eye movement analysis in simple visual tasks. *Computer Science and Information Systems, 19*(2), 619-637. https://doi.org/10.2298/CSIS210418065A

Contact information:

Qian WANG
(Corresponding author)
School of Electronic Information Engineering, Geely university of China, Chengdu, 641423
E-mail: wq_cduestc@163.com

Wei LI
School of Electronic Information Engineering, Geely university of China, Chengdu, 641423

Yuan-shuai LAN
School of Electronic Information Engineering, Geely university of China, Chengdu, 641423

Hua HE
School of Business Administration, Chongqing Technology and Business University, Chongqing, China, 400067